Supporting Information

Collisional Electron Transfer Route between Homogeneous Porphyrin Dye and Catalytic TiO_2/Re(I) Particles for CO_2 Reduction

Sunghan Choi,[†] Chul Hoon Kim,[†] Jin-Ook Baeg,[‡] Ho-Jin Son,[†,*] Chyongjin Pac,[†] and Sang Ook Kang[†,*]

[†]*Department of Advanced Materials Chemistry, Korea University, Sejong 30019, Korea*
[‡]*Artificial Photosynthesis Research Group, Korea Research Institute of Chemical Technology, Daejeon 34114, Korea*

*Correspondence and requests for materials should be addressed to
*E-mail: Ho-Jin Son: hjson@korea.ac.kr
*E-mail: Sang Ook Kang: sangok@korea.ac.kr

Table of contents

Sections	Titles	pages
Scheme S1	Synthetic route to **ZnP**.	S2
	Synthetic method and characterization of **ZnP**.	S2–S3
Figure S1	^{1}H-NMR spectroscopic view of **ZnP** in $CDCl_3$.	S4
Table S1	Crystal data and structure refinement for **ZnP**.	S5
Table S2	Bond lengths [Å] for **ZnP**.	S6
Table S3	Angles [°] for **ZnP**.	S7
Figure S2	The chemical structure of $\mathbf{ZnP_{CNPA}}$.	S8
Figure S3	Diffuse-reflectance spectra of $\mathbf{ZnP_{CNPA}}$/TiO_2/**ReP** powders and ATR-IR spectra of TiO_2/**ReP** powders before irradiation.	S9
Figure S4	Plots of CO formation versus irradiation time for **ZnP** + TiO_2/**ReP** in the presence of (0–15 vol%) water.	S10
Figure S5	^{13}C isotopic labelled experiments: GC spectrum of gas in the reaction vessel before and after photoreaction and MS spectra of each retention time.	S11
Figure S6	Stern−Volmer plot for emission quenching of **ZnP** by BIH.	S12
Table S4	Kinetic parameters of quenching of **ZnP** by BIH.	S13
Figure S7	Fluoroscence decay profiles of **ZnP** in the presence of either *x* mg TiO_2 (*x* = 0, 5 and 10) or 10 mg TiO_2/**ReP** particles in DMF.	S14
Table S5	Kinetic parameters of absorbance decay of $\mathbf{ZnP^{\bullet-}}$ in DMF.	S15
Figure S8	IR-SEC of **RePE** under different potential conditions.	S16
Figure S9	CVs of **RePE** in Ar and CO_2-saturated DMF/additive containing TBAP.	S17
Figure S10	Cross-sectional image and disassembled view of the IR-SEC cell.	S18
Figure S11	Disassembled view of the *in-situ* FTIR cell.	S19
Figure S12	Cross-sectional drawing of the *in-situ* FTIR cell.	S20
Table S6	FTIR assignments for key reaction intermediates of Re(I) complex based on the FTIR photolysis difference spectra and comparison with the literature values.	S21
Figure S13	FTIR spectra taken during the photocatalytic CO_2 to CO conversion.	S22
	References	S23

Scheme S1. Synthetic route to **ZnP**.[a]

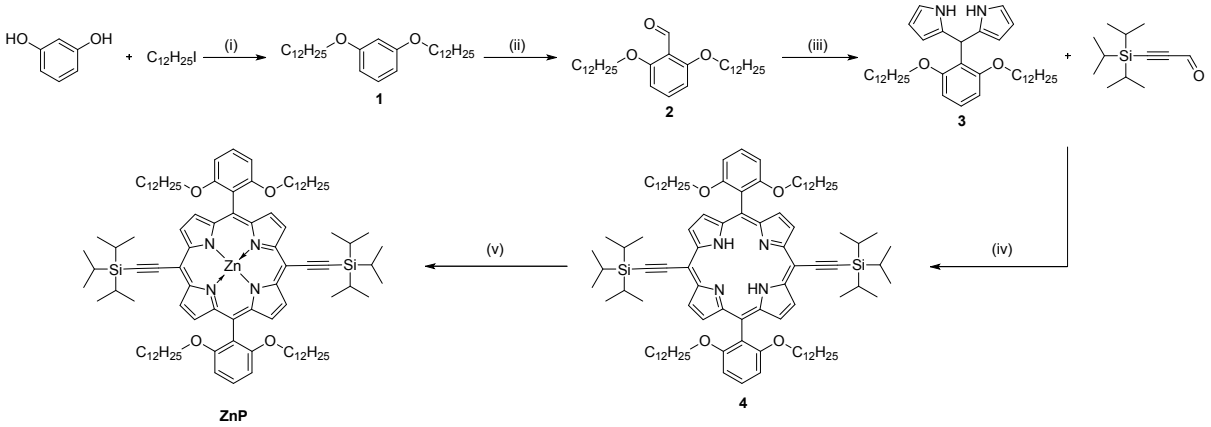

[a]Reagents and conditions: (*i*) KOH, DMSO, 80 °C, 8 h (70% yield); (*ii*) *n*-BuLi, TMEDA, DMF, THF, 0 °C, 3 h (65% yield); (*iii*) TFA, pyrrole, 25 °C, 2 h (35% yield); (*iv*) BF_3•Et_2O, DDQ, MC, 0 °C, 1 h (25% yield); (*v*) $Zn(OAc)_2$, $CHCl_3$, 70 °C, 6 h (99% yield).[S1]

Synthetic method and characterization of ZnP.

1,3-Di(dodecyloxy)benzene (1). Resorcinol (9 g, 81.8 mmol) and 1-iodododecane (45 mL) were successively added to a stirred suspension of potassium hydroxide (50 g, 900 mmol) in 200 mL of dimethyl sulfoxide (DMSO). The reaction was allowed to stir overnight at 80 ℃ and was then quenched with 400 mL of water. The product was extracted with dichloromethane (CH_2Cl_2), dried over magnesium sulfate ($MgSO_4$), and the solvent was evaporated under reduced pressure. The residue was purified by silica gel chromatography using hexane/ethyl acetate (15:1 *v*/*v*) as eluent to give 1,3-di(dodecyloxy)benzene (**1**) as a white solid (30 g, 82% yield). ^{1}H NMR ($CDCl_3$): δ 7.15 (t, J = 7.8 Hz, 1H), 6.49 (m, 3H), 3.92 (t, J = 6.3 Hz, 4H), 1.76 (m, 4H), 1.41 (m, 4H), 1.38–1.25 (m, 32H), 0.88 (t, J = 6.3 Hz, 6H).

2,6-Di(dodecyloxy)benzenaldehyde (2). A three-neck flask was fitted with a pressure-equalizing addition funnel and charged with **1** (30 g, 67.2 mmol) and tetramethylethylenediamine (TMEDA) (6 mL) in 200 mL of THF. The solution was degassed with a stream of N_2 for 15 min and cooled to 0 ℃. Under N_2, *n*-butyllithium (2.5 M solution in hexanes, 78 mmol) was added dropwise over 20 min and allowed to stir for 3 h. After warming to room temperature, dimethylformamide (DMF) (5.9 mL) was added dropwise, and the reaction was stirred for an additional 2 h. The reaction was quenched with water, and the

product was extracted with ether (3 × 150 mL), dried over $MgSO_4$, and the solvent was evaporated under reduced pressure. The residue was purified by silica gel chromatography using ethyl acetate/hexane (20:1 *v*/*v*) as eluent to give 2,6-di(dodecyloxy)benzenaldehyde (**2**) as a pale yellow solid (27 g, 85% yield). ^{1}H NMR ($CDCl_3$): δ 10.53 (s, 1H), 7.37 (t, J = 8.4 Hz, 1H), 6.52 (d, J = 8.4 Hz, 2H), 4.02 (t, J = 6.6 Hz, 4H), 1.80 (m, J = 6.6 Hz, 4H), 1.44 (m, 4H), 1.29–1.25 (m, 32H), 0.87 (t, J = 6.6 Hz, 6H).

***meso*-(2,6-Di(dodecyloxy)phenyl)dipyrromethane (3), 5,15-bis-[(trimethylsilanyl)ethynyl]-10,20-bis[2,6-di(dodecyloxy)phenyl]porphyrin (4), and [5,15-bis[(trimethylsilanyl)ethynyl]-10,20-bis[2,6-di(dodecyloxy)phenyl]porphinato]zinc (ZnP).** **2** (16 g, 33.7 mmol) was added to 55 mL of pyrrole and degassed for 10 min with a stream of N_2. Trifluoroacetic acid (0.3 mL) was then added in a portion, and the reaction mixture was stirred at room temperature for 2 h. NaOH (3 g, 75 mmol) was added to quench the reaction, followed by additional stirring for 1 h. The reaction mixture was filtered and the volatiles were evaporated from the filtrate using a rotary evaporator. The residue was subjected to column chromatography over silica gel chromatography using hexanes/ethyl acetate (15:1 *v*/*v*) to yield the desired product as a slightly yellow oil (5.5 g, 28%). Compound **3** was quickly used to prepare the next porphyrin molecule without further characterization due to its instability in the air. Compound **3** (5.5 g, 9.31 mmol) and trimethylsilylpropynal (1.7 mL, 9.31 mmol) were added to 1.5 L of dried CH_2Cl_2 and the solution was degassed for 5 min with a stream of N_2. BF_3-2•Et_2O (2.2 mL) was added slowly, and the reaction mixture was allowed to stir under N_2 atmosphere for 5 min at 0 ℃. Then 2 g of DDQ was added. After stirring for 30 min, 2 mL of pyridine was added. The precipitates were filtered off and the volatiles were removed under reduced pressure. The resulting residue was purified by silica gel column chromatography using hexane/dichloromethane (7:1 *v*/*v*) to afford pure 5,15-bis-[(trimethylsilanyl)ethynyl]-10,20-bis[2,6-di(dodecyloxy)phenyl]porphyrin (**4**), which was further metalated with zinc(II) acetate according to the literature procedure[S1] to afford [5,15-bis[(trimethylsilanyl)ethynyl]-10,20-bis[2,6-di(dodecyloxy)phenyl]porphinato]zinc (**ZnP**) as a deep green solid (1.45 g, 9.6% overall yield). ^{1}H NMR ($CDCl_3$): δ 9.66 (d, J = 6.0 Hz, 4H), 8.86 (d, J = 6.0 Hz, 4H), 7.67 (t, J = 6.0 Hz, 2H), 6.97 (d, J = 9.0 Hz, 4H), 3.81 (t, J = 6.0 Hz, 8H), 1.50–1.39 (m, 42H), 1.21–0.36 (m, 92H).

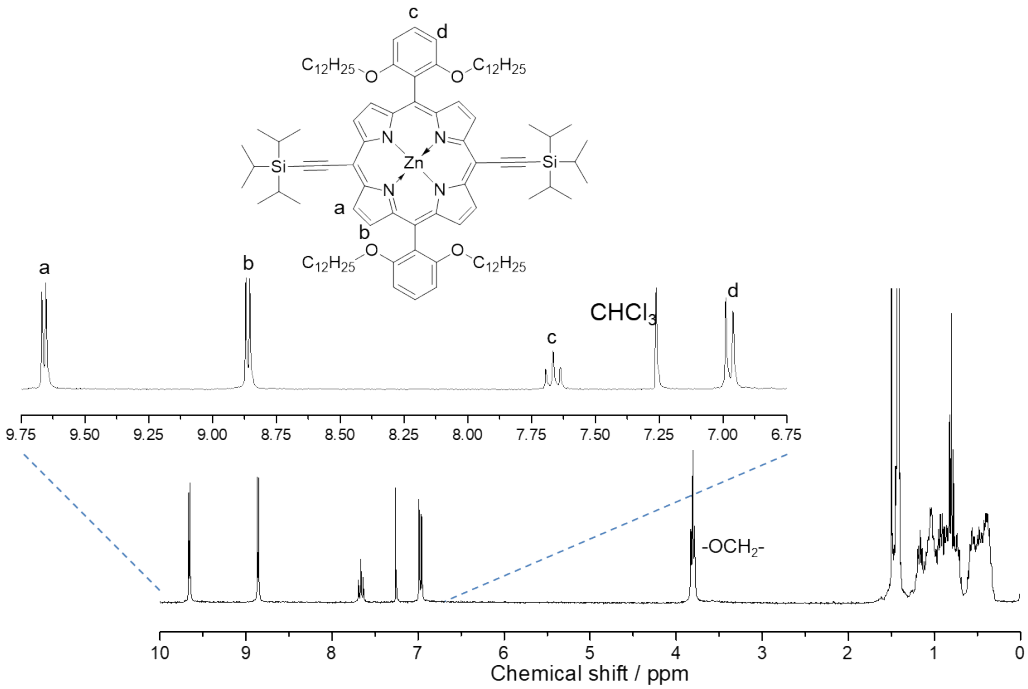

Figure S1. ^{1}H-NMR spectroscopic view of **ZnP** in $CDCl_3$.

Table S1. Crystal data and structure refinement for **ZnP**

Identification code	**ZnP** (CCDC 1901959)
Empirical formula	$C_{110}H_{172}ZnN_4O_6Si_2$
Formula weight	1768.15
Temperature	173(2) K
Wavelength	0.71073 Å
Crystal system, Space group	*Monoclinic*, *C*2/*c*
Unit cell dimensions	a = 38.361(3) Å
	b = 15.853(1) Å β = 100.831°
	c = 17.6645(1) Å
Volume	10550.9(1) Å^3
Z, D_{calc}	4, 1.110 Mg/cm^3
Absorption coefficient, μ	0.31 mm^{-1}
F(000)	3512
Crystal size	0.6 × 0.6 × 0.2 mm
θ range for data collection	1.755 to 25.374º
Limiting indices	$-46 \le h \le 46$, $-19 \le k \le 19$, $-21 \le l \le 21$
Reflections collected / unique	155444 / 9678 [R(int) = 0.1104]
Completeness to θ = 25.242	100.0%
Refinement method	Full-matrix least-squares on F^2
Data / restraints / parameters	9678 / 0 / 556
Goodness-of-fit on F^2	1.045
Final R indices [I > 2θ (I)]	$R_1{}^a$ = 0.0756, $wR_2{}^b$ = 0.1774
R indices (all data)	R_1 = 0.1237, wR_2 = 0.2241
Largest diff. peak and hole	1.181 and −0.926 e.Å^{-3}

$^aR_1 = \sum||F_o|-|F_c||$ (based on reflections with $F_o^2 > 2\sigma F^2$), $^bwR_2 = [\sum[w\,(F_o^2-F_c^2)^2] / \sum[w\,(F_o^2)^2]]^{1/2}$; $w = 1/[\sigma^2\,(F_o^2) + (0.095P)^2]$; $P = [\max(F_o^2, 0) + 2F_c^2]/3$(also with $F_o^2>2\sigma F^2$)

Table S2. Bond lengths [Å] for **ZnP**

Zn(1)-N(2)#1	2.05(3)	C(18)-C(19)	1.52(7)
Zn(1)-N(2)	2.05(3)	C(20)-C(19)	1.51(7)
Zn(1)-N(1)	2.05(3)	C(20)-C(21)	1.53(8)
Zn(1)-N(1)#1	2.05(3)	C(22)-C(23)	1.52(7)
Zn(1)-O(3)#1	2.32(3)	C(22)-C(21)	1.53(8)
Zn(1)-O(3)	2.32(3)	C(24)-C(23)	1.51(8)
Si(1)-C(42)	1.83(4)	C(24)-C(25)	1.53(7)
Si(1)-C(43)	1.88(5)	C(25)-C(26)	1.51(9)
Si(1)-C(49)	1.88(4)	C(28)-C(27)	1.52(1)
Si(1)-C(46)	1.88(5)	C(29)-C(30)	1.51(6)
O(1)-C(12)	1.37(5)	C(30)-C(31)	1.51(8)
O(1)-C(17)	1.42(5)	C(32)-C(33)	1.16(1)
O(2)-C(16)	1.37(5)	C(32)-C(31)	1.51(9)
O(2)-C(29)	1.42(6)	C(33)-C(34)	1.89(1)
O(3)-C(52)	1.38(5)	C(34)-C(35)	1.16(2)
O(3)-C(55)	1.39(6)	C(35)-C(36)	1.85(3)
N(2)-C(6)	1.37(5)	C(36)-C(37)	1.36(4)
N(2)-C(9)	1.37(5)	C(39)-C(40)	1.20(6)
N(1)-C(4)	1.35(5)	C(39)-C(38)	1.29(5)
N(1)-C(1)	1.38(5)	C(1)-C(10)#1	1.40(5)
C(5)-C(6)	1.40(6)	C(1)-C(2)	1.43(6)
C(5)-C(4)	1.42(5)	C(2)-C(3)	1.35(5)
C(5)-C(41)	1.43(6)	C(3)-C(4)	1.44(6)
C(6)-C(7)	1.44(5)	C(43)-C(45)	1.53(7)
C(7)-C(8)	1.34(6)	C(46)-C(48)	1.51(8)
C(8)-C(9)	1.43(5)	C(46)-C(47)	1.52(8)
C(9)-C(10)	1.40(6)	C(10)-C(11)	1.50(5)
C(41)-C(42)	1.21(6)	C(11)-C(16)	1.39(6)
C(44)-C(43)	1.53(7)	C(11)-C(12)	1.40(6)
C(50)-C(49)	1.54(7)	C(15)-C(16)	1.40(6)
C(51)-C(49)	1.53(7)	C(26)-C(27)	1.52(9)
C(13)-C(14)	1.37(7)	C(37)-C(38)	1.47(3)
C(13)-C(12)	1.36(5)	C(52)-C(53)	1.48(7)
C(14)-C(15)	1.38(6)	C(53)-C(54)	1.50(7)
C(17)-C(18)	1.51(7)	C(54)-C(55)	1.47(7)

Symmetry transformations used to generate equivalent atoms:
#1 -x+1/2,-y+1/2,-z

Table S3. Angles [°] for **ZnP**

N(2)#1-Zn(1)-N(1)	90(1)	C(29)-C(30)-C(31)	113(5)
N(2)-Zn(1)-N(1)	90(1)	C(33)-C(32)-C(31)	132(8)
N(2)#1-Zn(1)-N(1)#1	90(1)	C(32)-C(33)-C(34)	118(9)
N(2)-Zn(1)-N(1)#1	90(1)	C(35)-C(34)-C(33)	93(2)
N(2)#1-Zn(1)-O(3)#1	90(1)	C(34)-C(35)-C(36)	89(1)
N(2)-Zn(1)-O(3)#1	90(1)	C(37)-C(36)-C(35)	114(2)
N(1)-Zn(1)-O(3)#1	90(1)	C(40)-C(39)-C(38)	122(4)
N(1)#1-Zn(1)-O(3)#1	90(1)	N(1)-C(1)-C(10)#1	125(4)
N(2)#1-Zn(1)-O(3)	90(1)	N(1)-C(1)-C(2)	109(3)
N(2)-Zn(1)-O(3)	90(1)	C(10)#1-C(1)-C(2)	126(4)
N(1)-Zn(1)-O(3)	90(1)	C(3)-C(2)-C(1)	107(4)
N(1)#1-Zn(1)-O(3)	90(1)	C(2)-C(3)-C(4)	107(4)
C(42)-Si(1)-C(43)	108(2)	N(1)-C(4)-C(5)	125(4)
C(42)-Si(1)-C(49)	106(2)	N(1)-C(4)-C(3)	110(3)
C(43)-Si(1)-C(49)	110(2)	C(5)-C(4)-C(3)	125(4)
C(42)-Si(1)-C(46)	107(2)	C(41)-C(42)-Si(1)	173(4)
C(43)-Si(1)-C(46)	115(2)	C(45)-C(43)-C(44)	111(4)
C(49)-Si(1)-C(46)	111(2)	C(45)-C(43)-Si(1)	114(4)
C(12)-O(1)-C(17)	117(3)	C(44)-C(43)-Si(1)	114(4)
C(16)-O(2)-C(29)	118(3)	C(51)-C(49)-C(50)	110(4)
C(52)-O(3)-C(55)	112(4)	C(51)-C(49)-Si(1)	112(3)
C(52)-O(3)-Zn(1)	125(3)	C(50)-C(49)-Si(1)	112(3)
C(55)-O(3)-Zn(1)	124(3)	C(48)-C(46)-C(47)	112(5)
C(6)-N(2)-C(9)	107(3)	C(48)-C(46)-Si(1)	114(4)
C(6)-N(2)-Zn(1)	126(3)	C(47)-C(46)-Si(1)	114(5)
C(9)-N(2)-Zn(1)	127(3)	C(9)-C(10)-C(1)#1	126(3)
C(4)-N(1)-C(1)	106(3)	C(9)-C(10)-C(11)	116(3)
C(4)-N(1)-Zn(1)	127(2)	C(1)#1-C(10)-C(11)	117(4)
C(1)-N(1)-Zn(1)	127(3)	C(16)-C(11)-C(12)	119(4)
C(6)-C(5)-C(4)	127(4)	C(16)-C(11)-C(10)	121(4)
C(6)-C(5)-C(41)	116(3)	C(12)-C(11)-C(10)	120(4)
C(4)-C(5)-C(41)	117(4)	O(1)-C(12)-C(13)	124(4)
N(2)-C(6)-C(5)	125(3)	O(1)-C(12)-C(11)	116(3)
N(2)-C(6)-C(7)	109(3)	C(13)-C(12)-C(11)	120(4)
C(5)-C(6)-C(7)	126(4)	C(14)-C(15)-C(16)	119(4)
C(8)-C(7)-C(6)	108(4)	O(2)-C(16)-C(11)	115(3)
C(7)-C(8)-C(9)	107(3)	O(2)-C(16)-C(15)	124(4)
N(2)-C(9)-C(10)	126(3)	C(11)-C(16)-C(15)	121(4)
N(2)-C(9)-C(8)	110(4)	C(20)-C(19)-C(18)	113(4)
C(10)-C(9)-C(8)	125(4)	C(22)-C(21)-C(20)	115(5)
C(42)-C(41)-C(5)	176(5)	C(24)-C(23)-C(22)	114(5)
C(14)-C(13)-C(12)	120(4)	C(25)-C(26)-C(27)	113(6)
C(13)-C(14)-C(15)	121(4)	C(26)-C(27)-C(28)	113(7)
O(1)-C(17)-C(18)	108(3)	C(32)-C(31)-C(30)	115(7)
C(17)-C(18)-C(19)	111(4)	C(36)-C(37)-C(38)	119(2)
C(19)-C(20)-C(21)	114(4)	C(39)-C(38)-C(37)	123(3)
C(23)-C(22)-C(21)	113(5)	O(3)-C(52)-C(53)	108(4)
C(23)-C(24)-C(25)	114(5)	C(52)-C(53)-C(54)	105(4)
C(26)-C(25)-C(24)	114(6)	C(55)-C(54)-C(53)	106(5)
O(2)-C(29)-C(30)	107(4)	O(3)-C(55)-C(54)	108(4)

Symmetry transformations used to generate equivalent atoms:
#1 -x+1/2,-y+1/2,-z

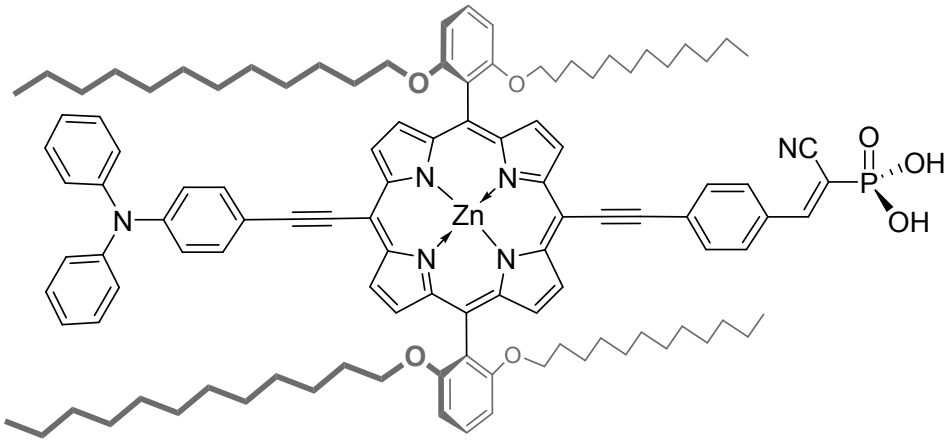

Figure S2. The chemical structure of $\mathbf{ZnP_{CNPA}}$.[S2]

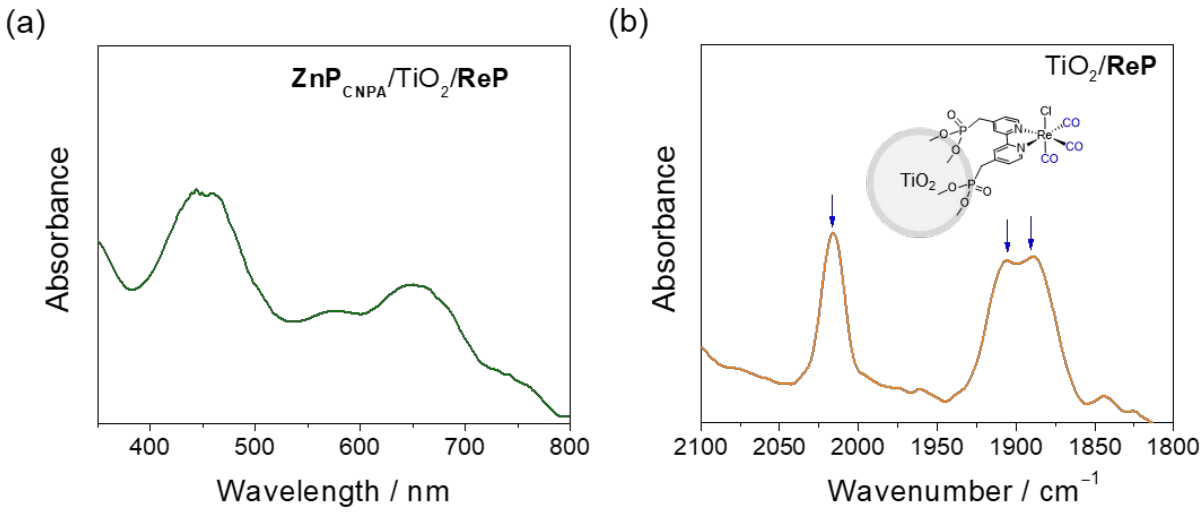

Figure S3. (a) Diffuse-reflectance spectra (DRS) of **ZnP$_{CNPA}$**/TiO$_2$/**ReP** powders and (b) ATR-IR spectra of TiO$_2$/**ReP**(0.1 μmol) powders before irradiation.

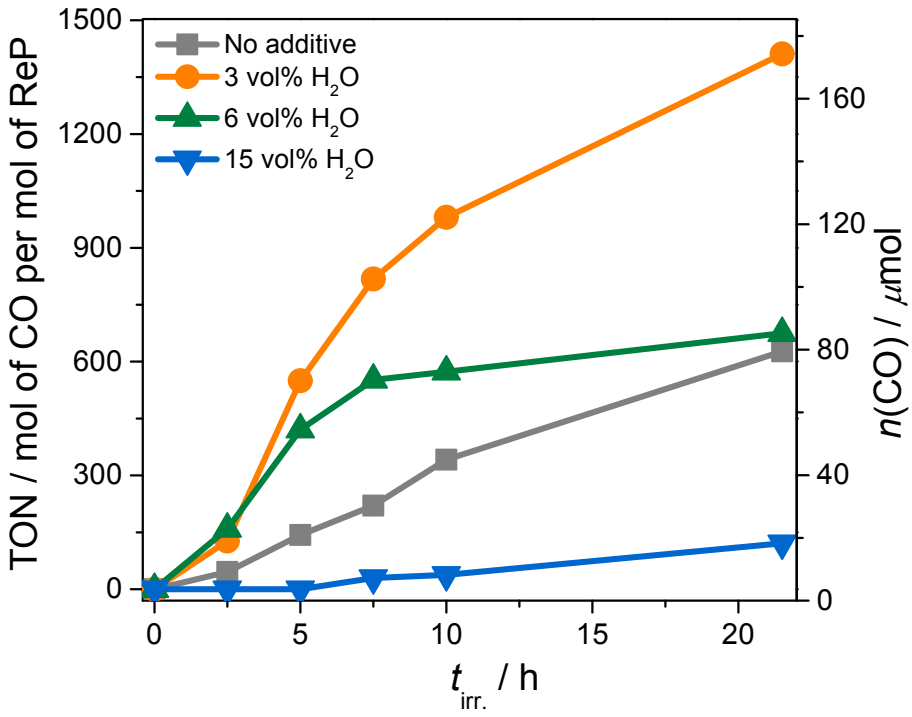

Figure S4. Plots of CO formation versus irradiation time for **ZnP** + TiO_2/**ReP** in the absence and presence of 3, 6, and 15 vol% H_2O in CO_2-saturated DMF containing 0.1 M BIH; irradiation at >500 nm. At 15 vol% H_2O, the relatively lower activity of binary hybrid is thought to be caused in part by the poor solubility of **ZnP** in reaction solvent containing the high water content.

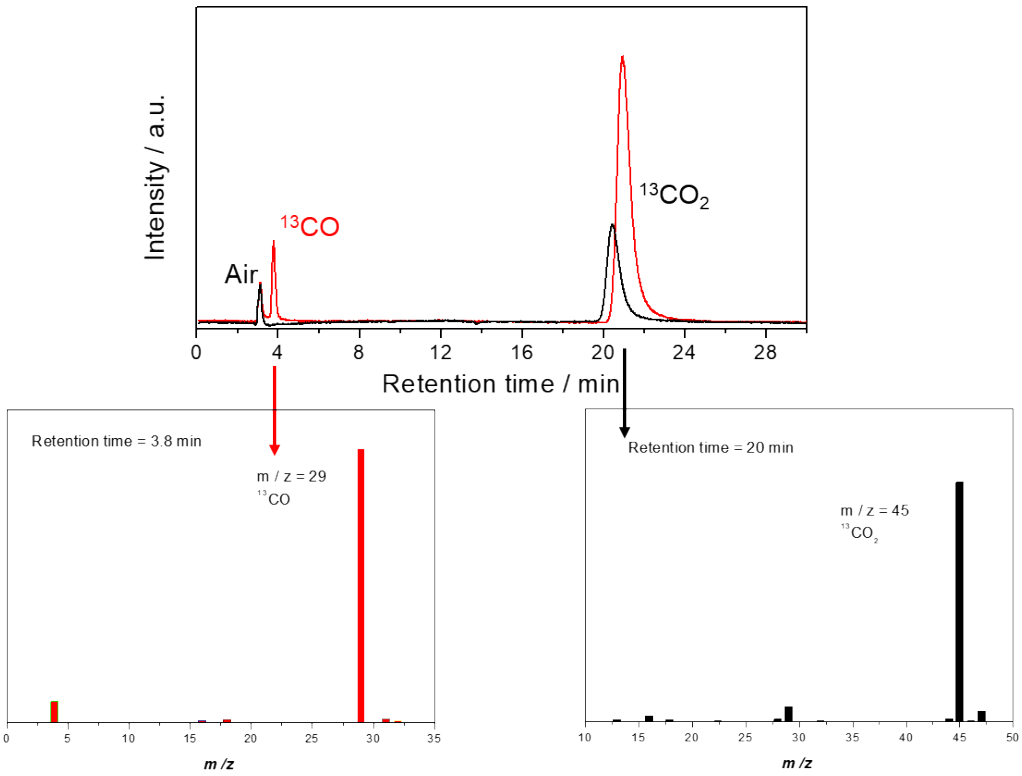

Figure S5. GC spectrum of gas in the reaction vessel before (black line) and after (red line) photoreaction and MS spectra of each retention time: GC-MS spectra was measured by Agilent Technologies 7890A GC equipped with 5975C inert MSD with Triple-Axis detector using a SUPELCO CarboxenTM 1010 PLOT Fused Silica Capillary column.

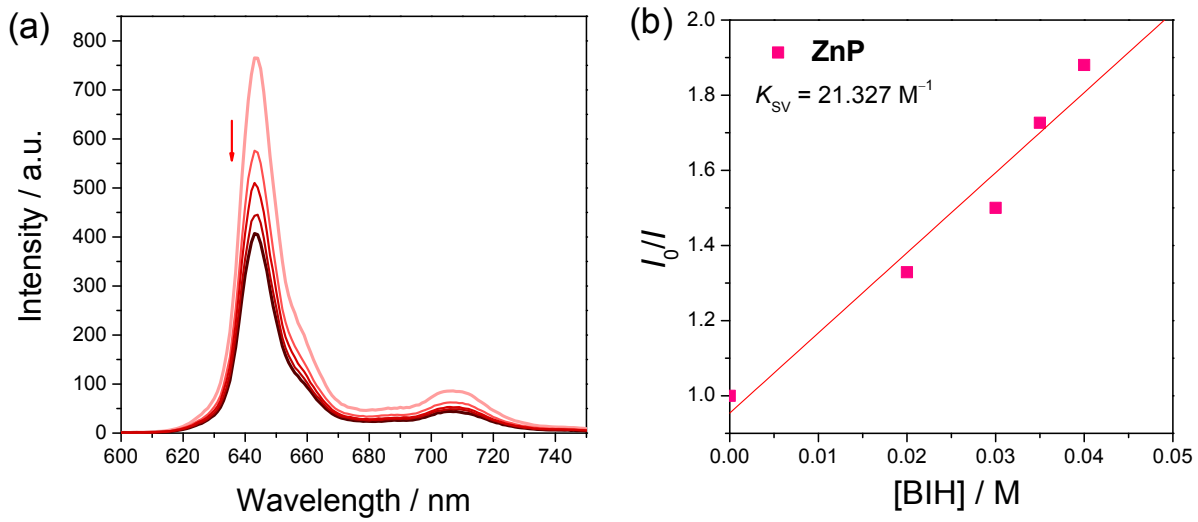

Figure S6. (a) PL intensity change of **ZnP** (2.5 μM) with varying BIH concentration. (b) Stern−Volmer plot for emission quenching (λ_{det} = 643 nm) of **ZnP** by BIH in N_2-degassed DMF; λ_{ex} = 440 nm.

Table S4. Kinetic parameters of emission quenching of **ZnP** by BIH in DMF.[a]

Sensitizer	K_{SV} (M^{-1})[b]	τ_0 (ns)[c]	k_q (10^9 M^{-1} s^{-1})[d]	Q[e]
ZnP	21.327	2.3	9.27	0.68

[a]Reaction condition: BIH + **ZnP** (2.5 μM) in DMF, λ_{ex} = 630 ± 20 nm. [b]Stern−Volmer quenching constant. [c]Fluorescence lifetime of the **ZnP** measured in an Ar-saturated DMF in the absence of BIH. [d]Quenching rate constant calculated using $k_q = K_{SV}/\tau_0$. [e]Quenching fraction (Q) in the presence of 0.1 M BIH, which was calculated as $0.1 \times K_{SV}/(1 + 0.1 \times K_{SV})$.[S3]

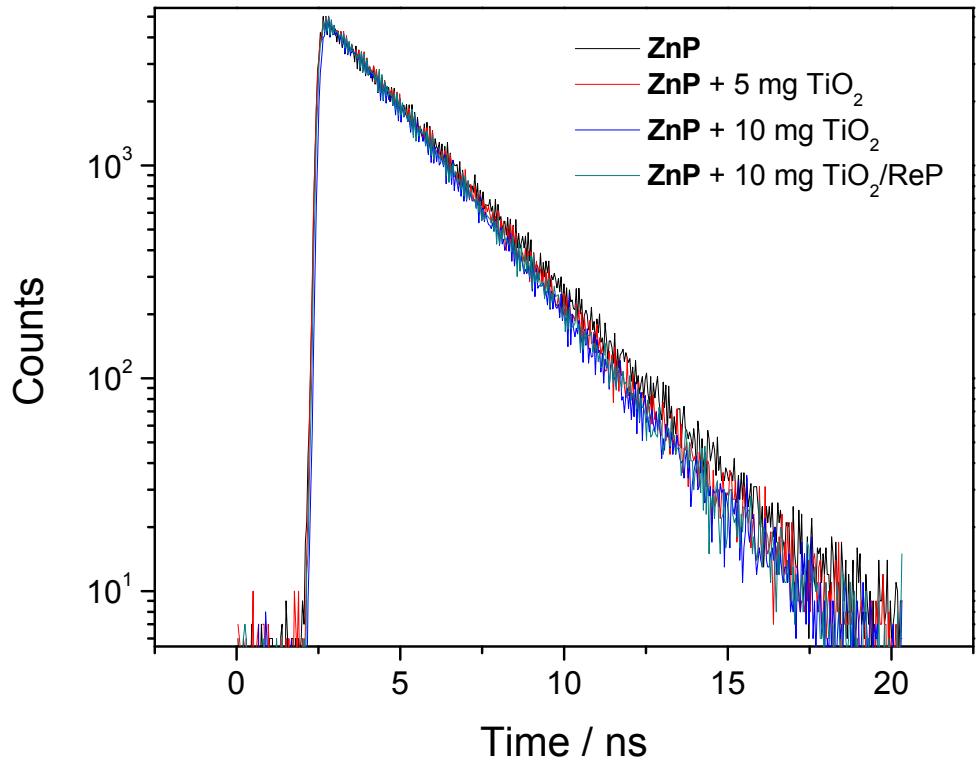

Figure S7. Fluoroscence decay profiles of **ZnP** in the presence of either *x* mg TiO_2 (*x* = 0, 5 and 10) or 10 mg TiO_2/**ReP** particles in DMF at room temperature. The dispersed TiO_2 particles were continuously stirred during measurement. These results indicate that the oxidative quenching pathway is not dominant in the hetero-binary system (**ZnP** + TiO_2/**ReP**); λ_{ex} = 440 nm.

Table S5. Kinetic parameters of absorbance decay of **ZnP**$^{\bullet-}$ in DMF.[a]

Photosensitizer	$t_{1/2}$ (min)[b]
ZnP	5.36
ZnP (with 1 mg TiO_2)	1.53
ZnP (with 1 mg TiO_2/**ReP**)	0.78
ZnP (with **RePE**)	1.01

[a]**ZnP**$^{\bullet-}$ had been generated by 5 min irradiation of an Ar-purged 4 mL DMF solvent containing 10 μM **ZnP** and 2.0 mM BIH in the absence or presence of quencher (1 mg TiO_2 particles, 1 mg TiO_2/**ReP** particles, or 2 μM **RePE**). [b]Half decay lifetimes of **ZnP**$^{\bullet-}$ absorbance decay (λ_{det} = 700 nm) traced in the dark with the variation of quenching source.

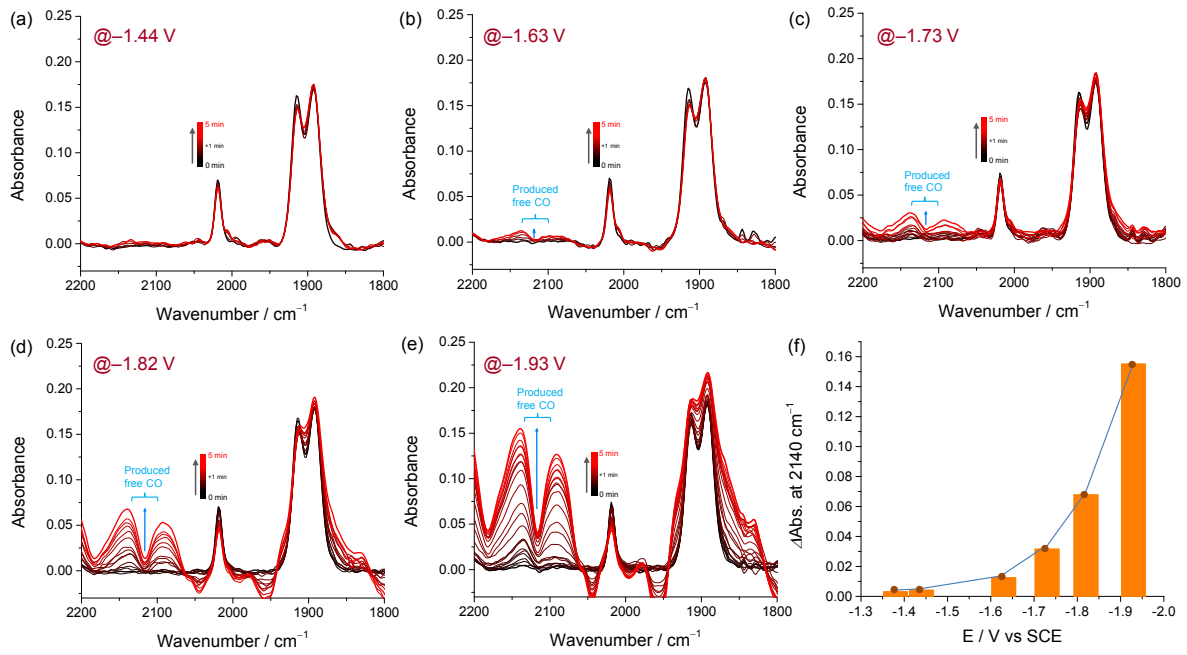

Figure S8. IR-SEC of **RePE** recorded for 5 min under different potential conditions (–1.44 to –1.93 V vs. SCE). Conditions: 0.1 mM **RePE**; CO_2-saturated DMF/TFE (3 vol% TFE) electrolyte solution (TBAP, 0.1 M); Pt working electrode, Pt counter electrode, and Ag pseudo-reference electrode.

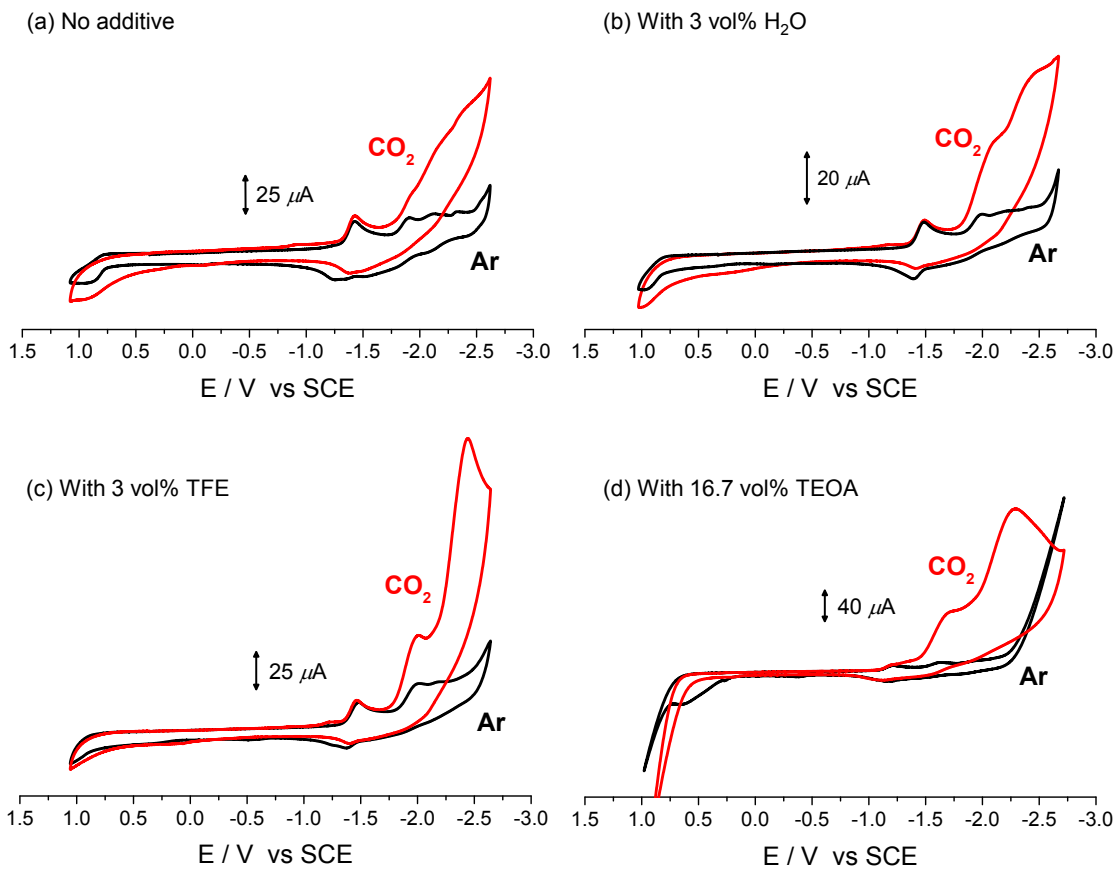

Figure S9. CVs of **RePE** (1 mM) in Ar and CO_2-saturated DMF/additive (additive = none, 3 vol% H_2O, 3 vol% TFE, and 16.7 vol% TEOA) containing 0.1 M TBAP at a scan rate of 100 mV/s. All potentials were measured with non-aqueous $Ag/AgNO_3$ reference electrode in Ar-saturated DMF electrolyte solution (TBAP, 0.1 M). For direct comparison with the reported literature values, the potentials were internally calibrated by using ferrocene/ferrocenium redox couple (Fc/Fc^+) and then converted to the SCE scale according to the following equation: $E(SCE) = E(Fc/Fc^+) + 0.38$ V.

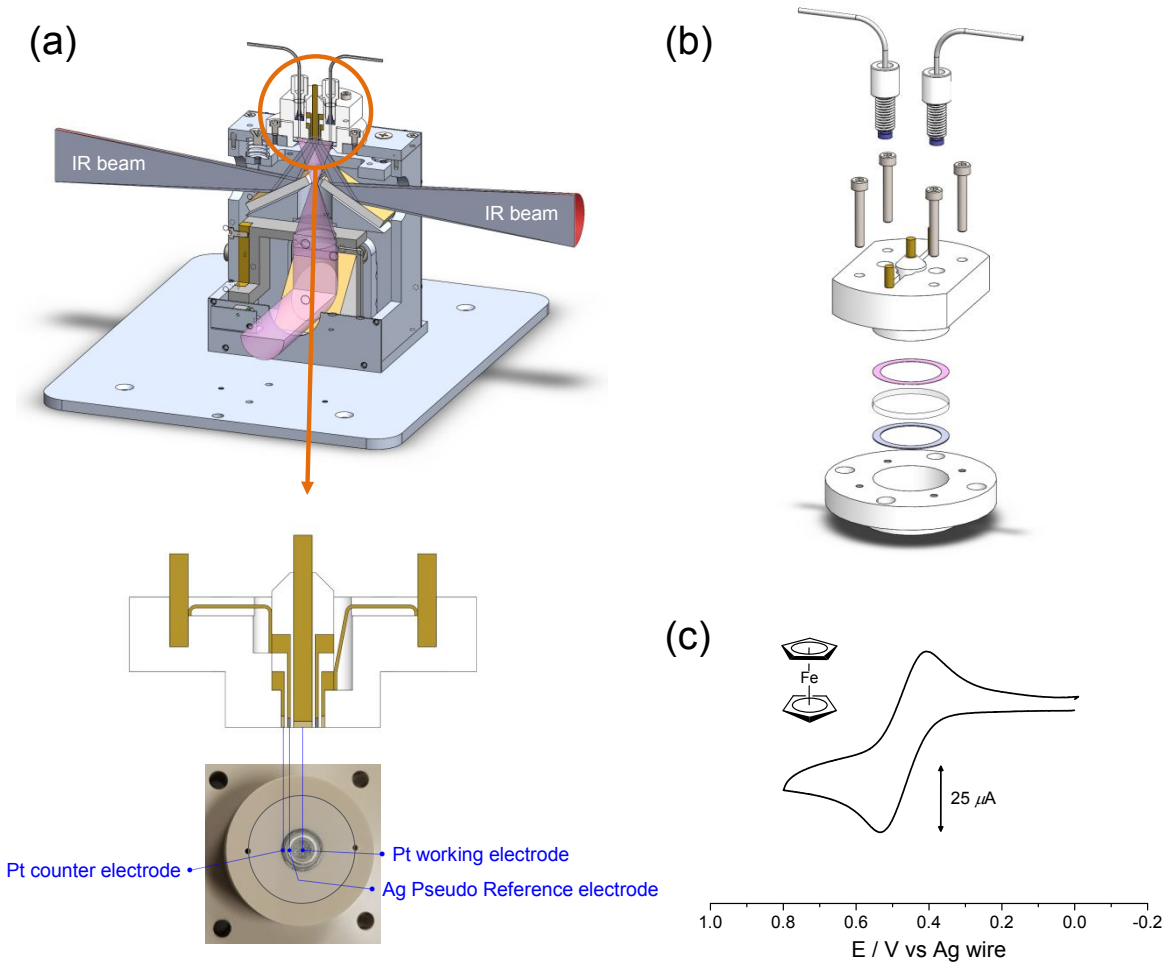

Figure S10. (a) Cross-sectional image (b) its disassembled view of IR-SEC cell. (c) CVs of the ferrocene in IR-SEC cell. Conditions: 0.01 mM ferrocene; 0.1 M TBAP/DMF; scan rate = 100 mV/s; working electrode = Pt; counter electrode = Pt; reference electrode = Ag. In this cell, a platinum (dia. 3.0 mm), platinum wire (dia. 7.0 mm, 0.5 mm thick), and Ag wire (dia. 5.0 mm, 0.5 mm thick) were used as the working electrode, counter electrode, and the pseudo-reference electrode, respectively.

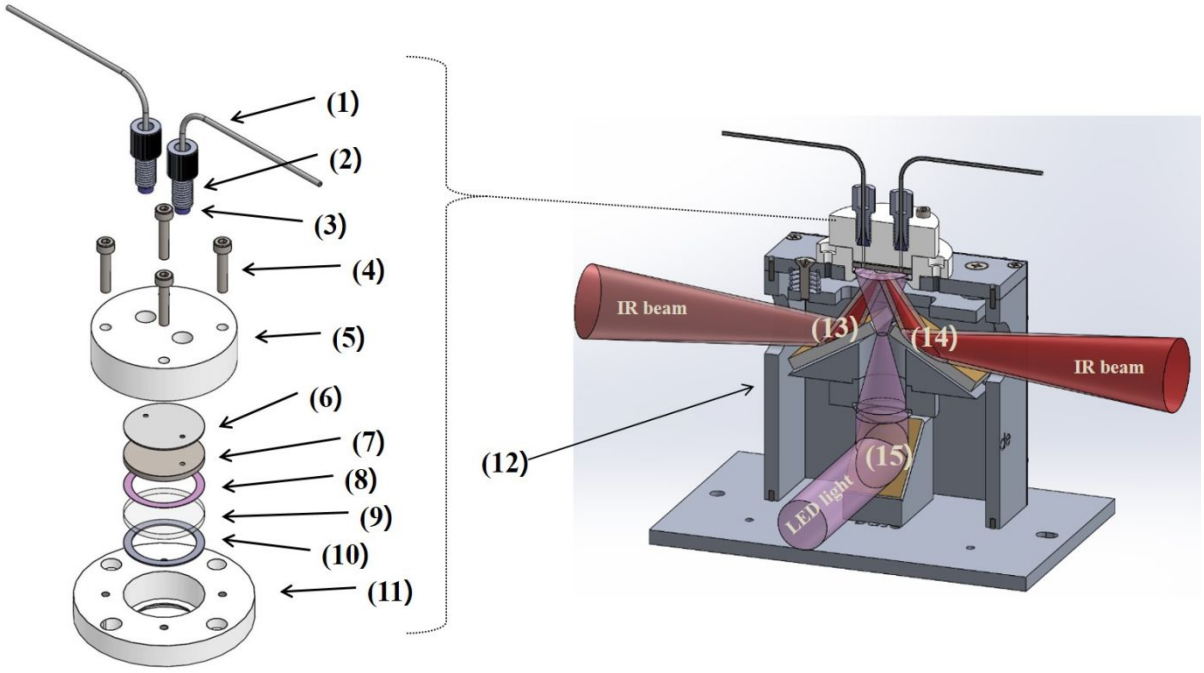

Figure S11. Disassembled view of the *in situ* FTIR cell. (1) Solution injection Tube (PTFE). (2) XP-230 PEEK fittings. (3) P-200 PTFE gasket. (4) M3 Hex Screw required to tighten the cell. (5) PEEK cell cover. (6) PEEK gasket for overflow prevention. (7) Sample plate for reflect IR beam. (8) Teflon spacer determines the path length (0.10 mm) of the cell. (9) Calcium fluoride window (OD25, T2mm). (10) PTFE gasket type ring. (11) Cell base body (PEEK). (12) Three mirror reflectance accessory. (13 to 15) Mirrors.

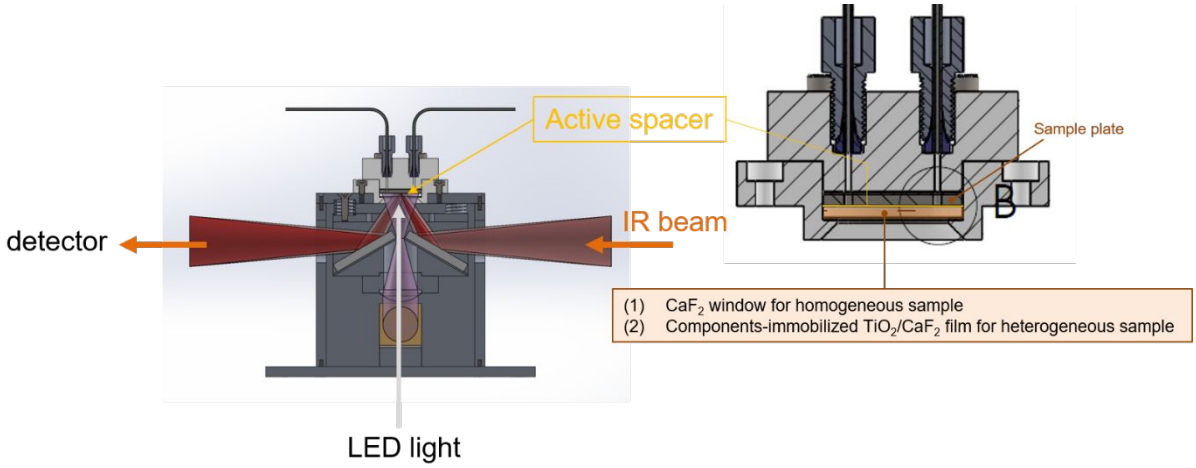

Figure S12. Cross-sectional drawing of the cell. The Teflon spacer, through which the IR-beam pass, has 0.10 mm pass length and 0.03 mL total volume.

Table S6. FTIR assignments for key reaction intermediates of Re(I) complex based on the FTIR photolysis difference spectra and comparison with the literature values.

This work[a]		the literature values	
ν(CO) / cm^{-1}	assignment	ν(CO) / cm^{-1}	assignment
2020(s), 1914(s), 1892(s)	LReCl (**ReP**)	2018, 1911, 1890[S4]	Re(dmb)(CO)$_3$Cl[b]
1994, 1881, 1861	LReCl$^{\bullet-}$ (OERS)	1994, 1880, 1862[S5]	[Re(bpy)(CO)$_3$Cl]$^{\bullet-}$
1983, 1866, 1850	LRe$^{\bullet}$(17 electron species)	1983, 1865, 1850[S6]	[Re(bpy-^{t}Bu)(CO)$_3$]$^{\bullet}$[c]
2009, 1898	L$^{\bullet-}$Re^{I} (Re-DMF)	2007, 1897(br)[S4]	[Re(dmb)(CO)$_3$(THF)][b]
1936, 1830	LRe:$^-$ (2e$^-$ reduced species)	1938, 1832[S4]	[Re(dmb)(CO)$_3$]$^-$[b]
2004, 1894	LRe-COOH	2005, 1895[S4]	[Re(dmb)(CO)$_3$(COOH)][b]

[a]The FTIR assignments are performed based on the literature values. [b]dmb = 4,4′-dimethyl-2,2′-bipyridine. [c]bpy-^{t}Bu = 4,4′-di-*tert*-butyl-2,2′-bipyridine.

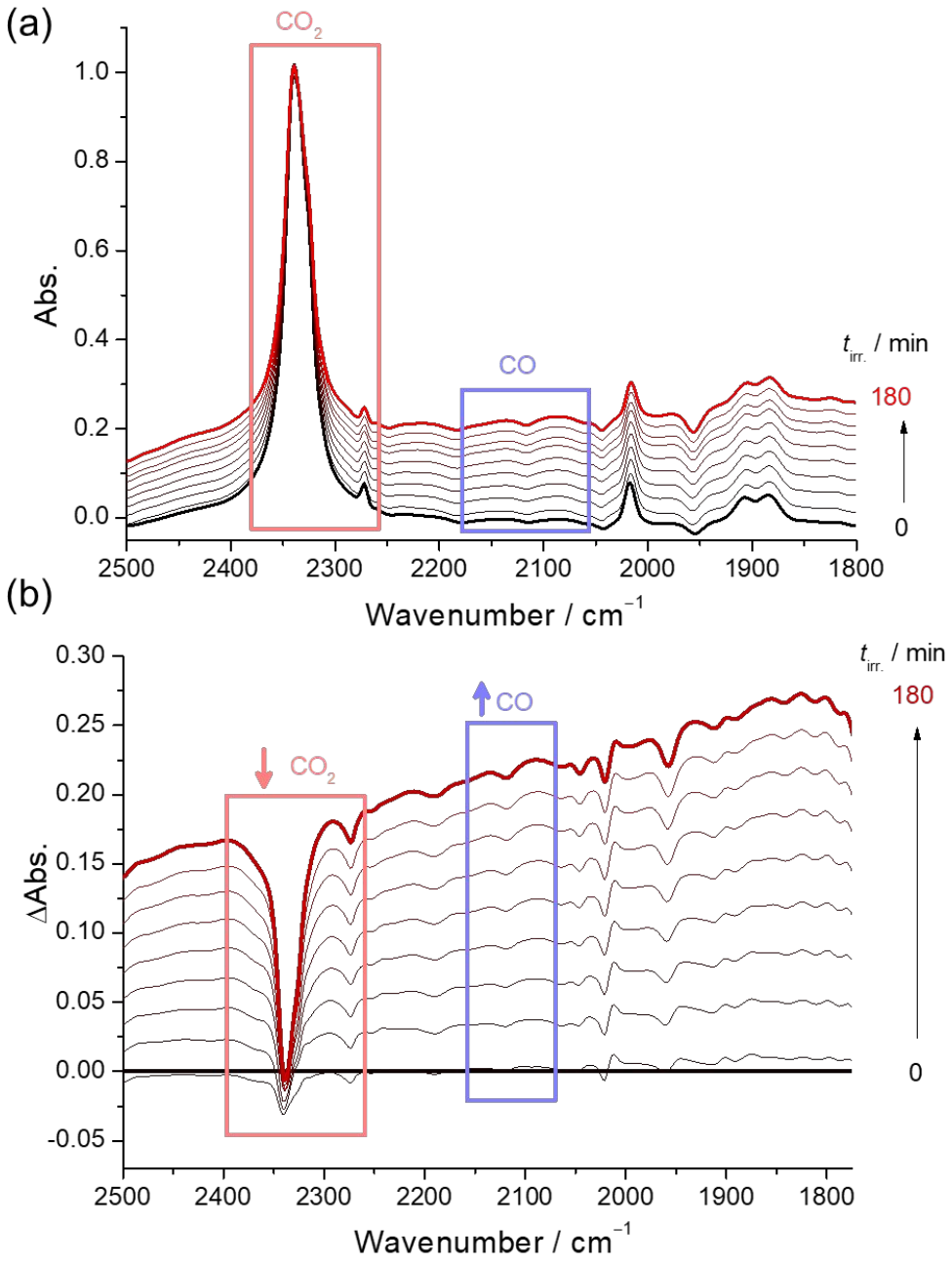

Figure S13. (a) FTIR spectral changes following irradiation time and (b) FTIR difference spectra for free CO peak (ν(CO) = 2140 cm^{-1}) for TiO_2/**ReP** mesoporous film on a CaF_2 plate with loaded amounts of **ReP** corresponding to 0.42 μmol per 10 mg of TiO_2; the sample plate dipped in 0.03 mL of CO_2-saturated DMF containing 0.5 mM **ZnP** and 0.10 M BIH was irradiated at λ >495 nm by using an LED lamp at 298 K.

References

[S1] Lee, C. Y.; Hupp, J. T. Dye Sensitized Solar Cells: TiO_2 Sensitization with a Bodipy-Porphyrin Antenna System. *Langmuir* **2010**, *26*, 3760−3765.

[S2] Won, D.-I.; Lee, J.-S.; Ba, Q.; Cho, Y.-J.; Cheong, H.-Y.; Choi, S.; Kim, C. H.; Son, H.-J.; Pac, C.; Kang, S. O. Development of a Lower Energy Photosensitizer for Photocatalytic CO_2 Reduction: Modification of Porphyrin Dye in Hybrid Catalyst System. *ACS Catal.* **2018**, *8*, 1018–1030.

[S3] Su, Y.; Kuijpers, K. P. L.; König, N.; Shang, M.; Hessel, V.; Noël, T. A Mechanistic Investigation of the Visible Light Photocatalytic Trifluoromethylation of Heterocycles using CF_3I in flow. *Chem. Eur. J.* **2016**, *22*, 12295−12300.

[S4] Hayashi, Y.; Kita, S.; Brunschwig, B. S.; Fujita, E. Involvement of a Binuclear Species with the Re−C(O)O−Re Moiety in CO_2 Reduction Catalyzed by Tricarbonyl Rhenium(I) Complexes with Diimine Ligands: Strikingly Slow Formation of the Re−Re and Re−C(O)O−Re Species from $Re(dmb)(CO)_3S$ (dmb = 4,4′-Dimethyl-2,2′-bipyridine, S = Solvent). *J. Am. Chem. Soc.* **2003**, *125*, 11976−11987.

[S5] Johnson, F. P. A.; George, M. W.; Hartl, F.; Turner, J. J. Electrocatalytic Reduction of CO_2 Using the Complexes $[Re(bpy)(CO)_3L]^n$ (n = +1, L = $P(OEt)_3$, CH_3CN; n = 0, L = Cl^-, Otf^-; bpy = 2,2′-Bipyridine; Otf^- = CF_3SO_3) as Catalyst Precursors: Infrared Spectroelectrochemical Investigation. *Organometallics* **1996**, *15*, 3374−3387.

[S6] Smieja, J. M.; Kubiak, C. P. Re(bipy-^{t}Bu)$(CO)_3$Cl–improved Catalytic Activity for Reduction of Carbon Dioxide: IR-Spectroelectrochemical and Mechanistic Studies. *Inorg. Chem.* **2010**, *49*, 9283−9289.